Postprocesses in tubular electrospun nanofibers

A. Arinstein[1,2] and E. Zussman[2]
[1]*Department of Physics, Bar-Ilan University, Ramat-Gan 52900, Israel*
[2]*Department of Mechanical Engineering, Technion–Israel Institute of Technology, Haifa 32000, Israel*
(Received 6 August 2007; published 9 November 2007)

The postprocesses that occur in coelectrospun polymer nanofibers are investigated. The high rate of solvent evaporation during the electrospinning of fibers results in such a rapid formation of the shell of the tubular nanofibers, that the polymer molecules composing the fibers are in a nonequilibrium state. This stretched state of macromolecules is assumed to be stabilized in a solid matrix, and can account for the anomalous properties of the nanofibers. During this processing stage a considerable amount of solvent remains inside the tubular nanofibers. The evaporation of the solvent continues for several minutes, and is accompanied by further evolution of the nanofibers in both their microstates and macrostates. In this paper, we examine possible macrostate modifications of the nanofibers, such as radial buckling. The theoretical model which describes the kinetics of the solvent evaporation is found to be in good agreement with experimental observations. Thus, the physical parameters of the system in question can be estimated, and the conditions of fiber shell instability that produce buckling of the tubular nanofibers can also be predicted.

DOI: 10.1103/PhysRevE.76.056303 PACS number(s): 47.61.−k, 81.05.Lg, 81.16.−c

I. INTRODUCTION

Electrospinning is a commonly used process for fabricating polymer-based nanofibers [1–4]. In this process, a polymer solution is extruded from a spinneret, and in the presence of a sufficiently strong electric field, a jet is formed at the tip. This jet then undergoes extreme elongation thereby stretching the polymer molecules within it. As this is occurring, the rapid solvent evaporation fixes the polymer matrix in this stretched, yet nonequilibrium state. This process allows for the fabrication in a single stage and in less than 10 ms, of nanofibers ranging from 100 to 1000 nm in diameter. The morphology and mechanical properties of the collected fibers are commonly studied by focusing on the parameters of the electrospinning process [5–9]. Many studies have examined polymer rheology [10], while others have focused on controlling the electrostatic field, or determining the effect of various setup configurations [11]. However, the effect of the evaporation rate on the physical features of the electrospun fibers has not been studied in detail.

The very rapid evaporation process is a challenging problem for experimental investigation. However, theoretical analysis and computer simulations can clarify some aspects of the problem in question. For example, the role that the high evaporation rate plays in the fabrication of polymeric electrospun nanofibers has already been discussed by Koombhongse *et al.* [12] and treated quantitatively by Guenthner *et al.* [13]. In particular, it was demonstrated that when the evaporation is very fast, the polymer density at the fiber/vapor interface increases sharply, thus creating a polymer density gradient that acts as a barrier, or skin, that resists further solvent evaporation.

These results are in good agreement with our presumption that despite the rapid evaporation that has occurred, the collected electrospun nanofibers still contain a significant amount of solvent. The presence of the solvent, which now evaporates even slower due to the barrier that has formed, apparently results in "relaxation" of the fabricated nanofibers. This relaxation causes certain postprocesses to take place within the system. Therefore, the effect of this residual solvent is crucial to understanding the mechanisms that affect the nanofibers' mechanical properties, and provides the motivation for the presented work.

The structure of this paper is as follows: First, we describe the experimental system which was designed to allow us to observe the evaporation kinetics within the tubular electrospun nanofibers containing the solvent. Next, we propose a physical model of the processes observed in the experiments. Based on this model and the experimental observations, we are able to elucidate the effect of some of the system parameters. Finally, we discuss one of the possible phenomena which occurs as a result of solvent evaporation, i.e., the radial buckling of nanofibers, which is occasionally observed in our experimental system.

II. EXPERIMENTAL SYSTEM

As mentioned above, the investigation of the very rapid solvent evaporation occurring in the electrospinning process is a complex experimental problem. Therefore, we focus on a special case of the system discussed by Guenthner *et al.* [13]. Their theoretical analysis and simulation have shown that the polymer molecules in the electrospun fibers are inhomogeneously distributed in the cross section of the nanofiber, forming a compact surface or "shell." Also, a spongy core is formed as a result of the entrapped solvent which cannot quickly escape, due to the low penetrability of the formed shell. Clearly, a tubular nanofiber filled with solvent can be considered as a special case of the Guenther *et al.* system. In our experimental system, we used tubular nanofibers, thereby enabling us to observe the decrease in the amount of solvent inside the nanofibers due to evaporation. In this manner, we are able to track the kinetics of solvent evaporation through the shell.

The method of fabricating such tubular nanofibers is presented in detail in Ref. [14]. Briefly, two polymer solutions

 ©2007 The American Physical Society

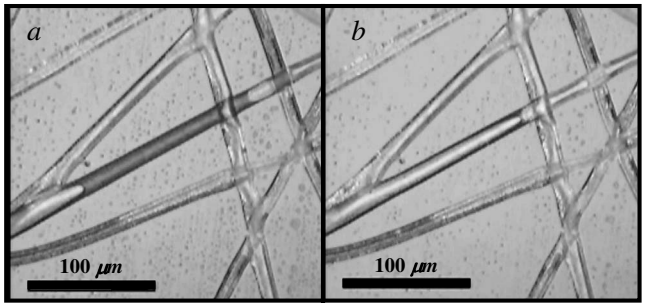

FIG. 1. (a) A typical image of an as-spun fiber with an entrapped slug bounded by two menisci and (b) disappearance of this slug as a result of solvent evaporation.

are supplied from a spinneret consisting of two coaxial capillaries. Close to the spinneret's exit, the emerging jet has a cross section composed of two concentric layers, which forms a core shell structure. The outer surface of the shell experiences a dry spinning process, as it is exposed to the surrounding air. Thus, the solvent diffusion and the evaporation at the fiber/vapor interface promote solidification and the resultant morphology at the outer surface. On the other hand, the inner layer of the shell experiences a wet spinning process, as it is in contact with the relatively nonvolatile core solution (e.g., aqueous solution) which is a nonsolvent to the polymer shell. The core solution can then be regarded as a coagulation bath for the shell.

Experimental observations. The collected tubular nanofibers with the entrapped core solvent were observed using an optical microscope immediately after their fabrication, enabling the experimental analysis of further evolution of the system in question. This process has a typical time duration of tens of seconds, which means that while the initial stage could not be observed, some deductions regarding it can be formulated from subsequent developments and an analysis of the entire process (see Sec. IV B below). Subsequent experimental observations of the as-spun nanofibers reveal that they consist of microtubes containing many slugs of entrapped core solvent that are bound by a vapor phase. A typical image of an as-spun fiber with an entrapped slug bound by two menisci is depicted in Fig. 1(a). The observed slug shortens as evidenced by the menisci coming towards each other at a velocity V_m and finally disappears as a result of solvent evaporation [see Fig. 1(b)]. Typical patterns of meniscus displacement and its velocity V_m are displayed in Fig. 2. Initially, the meniscus moves at a constant rate (see the inset in the graph for the pattern of a long slug), then its velocity slows down, and finally, when the distance between the left and right menisci of the liquid is small, the meniscus displacement tapers off slowly. When the entire slug has eventually evaporated, we are left with a hollow.

It is clear that the menisci motion is caused by the solvent evaporating, so if a relationship between these processes can be found, it will assist in studying the evaporation kinetics of the as-spun nanofibers. Note that the typical evaporation time of the core solvent is in the order of tens of seconds. For this reason, along with the observations described above, one can conclude that relaxation and the further evolution of the polymeric matrix takes place inside the nanofibers after their formation.

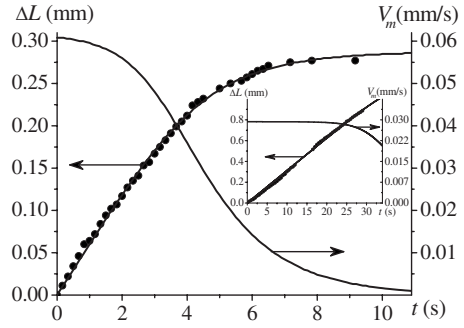

FIG. 2. The meniscus displacement $\Delta L(t)=L_0-L_{\mathrm{cap}}(t)$ (left axis) and its rate (right axis) vs time. The dots display the experimental data and the lines display the theoretical model. The inset displays another set of experimental data for which evaporation through the capillary wall is dominant.

III. PHYSICAL MODEL OF THE SYSTEM

As the solvent evaporation results in a decrease of the liquid quantity inside the fibers, this has a direct correlation with the menisci motion. Therefore, by studying the menisci displacement pattern, we can clarify the processes accompanying the solvent evaporation.

A. Preliminary estimates

A reasonable starting point is to consider the dominant processes affecting the evaporation kinetics (see Fig. 3 with a schematic description of this process). The evaporation of the core solvent can take place at both the shell and the menisci. At first glance, it would appear that the latter channel would be dominant, since the filtration of solvent through the capillary wall is limited by a very low diffusion coefficient ($D_s \propto 10^{-13}-10^{-12}$ m^2/s [15]). However, taking into account the ratio of surface areas of the meniscus and capillary wall, it is found that solvent evaporation from the meniscus surfaces has a limited influence on the evaporation kinetics, and that solvent filtration through the capillary wall controls the process in question. Indeed, the characteristic time of the solvent evaporation from the meniscus t_m can be approximated as

$$t_m \propto D_g^{-1}(2L_0C_l/C_g)^2 \approx 4\times 10^4 \text{ s}, \tag{1}$$

where D_g ($D_g \propto 10^{-5}$ m^2/s) and C_g are the diffusion coefficient and solvent density in the gas phase, C_l is the density of liquid solvent ($C_l/C_g \propto 10^3$), and L_0 is half of the initial length of the slug ($L_0 \approx 3\times 10^{-4}$ m).

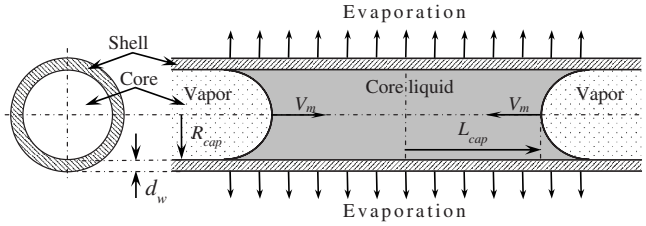

FIG. 3. A scheme of the dominant processes determining the evaporation kinetic.

This calculated time duration exceeds the experimentally observed time of the evaporation process by two and a half orders of magnitude. Even if such a difference seems to be negligible, one should take into account that the above value is underestimated. The reason is that the evaporated gas is assumed to be removed without any impediments. In reality, outgas can occur only through the tube shell, and if we take this into account, we come up with a dramatic increase in the evaporation time (and if the concentration of evaporated gas manages to equal the saturated concentration, the process can stop altogether).

However, the most cogent argument supporting the negligibility of solvent evaporation from the meniscus surfaces is that the evaporation time is dependent on the displacement rate of the menisci. According to experimental observation, if the length of a slug is long enough, the displacement rate of the meniscus is nearly constant (see the inset in Fig. 2), and decreases exponentially when the length of the slug becomes short enough (see Fig. 2). However, the solvent evaporation from the meniscus surfaces results in other dependence of type of inverse square root $V_m(t) \propto \sqrt{1/t}$. Therefore, the kinetics of the process in question cannot be explained by solvent evaporation from the meniscus surfaces, but only by infiltration of the solvent through the capillary wall and its subsequent evaporation at the fiber-vapor interface (the last process occurs very quickly).

The time necessary for the infiltration of the liquid solvent through the wall of a capillary can be determined by considering the flux of the liquid that read

$$2\pi R_{\mathrm{cap}} 2L_0 D_s (\partial C_l/\partial r) t_w \propto 2\pi R_{\mathrm{cap}} 2L_0 D_s (C_l/d_w) t_w = \pi R_{\mathrm{cap}}^2 2L_0 C_l, \tag{2}$$

where R_{cap} and d_w are the radius of a capillary and thickness of its walls, respectively.

Assuming $D_s \propto 10^{-13}$ m^2/s, $R_{\mathrm{cap}} \propto 10^{-5}$ m, and $d_w \propto 0.5 \times 10^{-6}$ m, then

$$t_w \propto R_{\mathrm{cap}} d_w / D_s \approx 1 \text{ min}. \tag{3}$$

This time scale is in good agreement with the experimentally observed duration of the evaporation process. Therefore, we can conclude that the dominant process determining the rate of menisci recession is infiltration through the wall of the capillary by the liquid solvent and its subsequent evaporation. Therefore, from this point on, we will deal exclusively with this process and disregard evaporation through the menisci.

B. Problem formulation

Our aim is to determine the entrapped slug's evolution and its evaporation through the shell over time. According to experimental observations no deformations of most of capillaries accompany the solvent evaporation. Hence a pressure inside of capillary is decreasing, and this gradient of pressure results in a solvent flow directed from meniscus to the center of a slug, compensating the solvent evaporation inside of capillary. Since the length of the slug is much larger than its radius, $L \gg R_{\mathrm{cap}}$ and Reynolds number, $\mathrm{Re} = C_l R_{\mathrm{cap}} V_m / \eta \propto 10^{-6}$, is very low, locally we can assume Poiseuille's flow

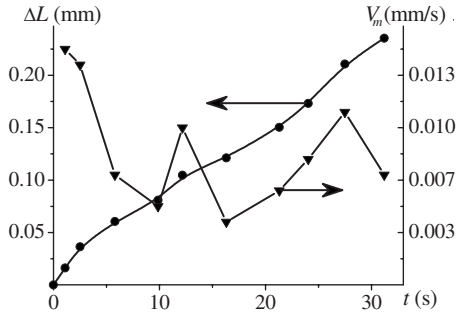

FIG. 4. The meniscus displacement $\Delta L(t) = L_0 - L_{\mathrm{cap}}(t)$ (left axis) and its rate (right axis) vs time in the case of deformed capillaries.

$$V(x,t) = -\frac{R_{\mathrm{cap}}^2}{8\eta} \frac{\partial P(x,t)}{\partial x}, \tag{4}$$

where $V(x,t)$ is the mean velocity of solvent in cross-section of capillary and η is the solvent viscosity.

The second equation describing the process incorporates the mass conservation law which takes into account the solvent evaporation

$$\frac{\partial V(x,t)}{\partial x} = -\frac{2D_s}{R_{\mathrm{cap}} d_w} \frac{1 + aP(x,t)/P_b}{1+a}. \tag{5}$$

The key point of this equation is that the liquid flux through the capillary wall varies along the capillary. The reason for this is that a decrease in pressure along the capillary hampers the infiltration of the fluid through the wall of capillary. This fact was taken into account in the simplest manner, by representing the pressure drop using a linear function which equals 1 when $x = L_{\mathrm{cap}}(t)$, with a single free parameter a.

The boundary conditions for Eqs. (4) and (5) are

$$P(x,t)|_{x=\pm L_{\mathrm{cap}}(t)} = P_{\mathrm{at}} - \frac{2\gamma}{R_{\mathrm{cap}}} = P_b,$$

$$V(x,t)|_{x=\pm L_{\mathrm{cap}}(t)} = \pm \frac{\partial L_{\mathrm{cap}}(t)}{\partial t}, \tag{6}$$

$$L_{\mathrm{cap}}(t=0) = L_0,$$

where $P_{\mathrm{at}} = 10^5$ N/m^2 is the atmosphere pressure and γ is the surface tension coefficient.

Assuming $\gamma \propto 50 \times 10^{-3}$ N/m and $R_{\mathrm{cap}} \propto 2 \times 10^{-5}$ m, then $2\gamma/R_{\mathrm{cap}} \propto 0.1 \times 10^5$ N/m^2 ($\sim 0.1 P_{\mathrm{at}}$), thus we can conclude that the influence of the surface tension on the process' kinetics is negligible. However, in the case of radial deformation of the capillary (e.g., due to bending) the influence of surface tension can become significant and result in a decrease of the displacement rate of the meniscus. Such phenomena were observed experimentally (see Fig. 4).

IV. THE KINETICS OF SOLVENT EVAPORATION

Equations (4) and (5), together with the boundary conditions (6), allow us to more fully investigate the evaporation

process and the fiber's evolution. In particular, we can determine the pressure distribution along the fiber, which provides information about the elastic energy being stored in the fibers during evaporation as a result of their radial compression. This elastic energy accounts for additional phenomena observed in the experiments, for example, the formation of gas bubbles in the fibers, or modifications in the fiber structure, such as buckling. Also, the velocity distribution along the fiber allows us to analyze the displacement rate of the menisci being observed experimentally. Correlating the experimental observations with the above model provides us with the actual physical parameters of the fibers.

A. The pressure and velocity distribution

The solution of Eqs. (4) and (5) can be obtained as follows: after the differentiation of Eq. (5) and substitution of $\partial P/\partial x$ in Eq. (4) we obtain

$$\xi^2 \frac{\partial^2 V(x,t)}{\partial x^2} - V(x,t) = 0 \tag{7}$$

and the velocity is

$$V(x,t) = -A(t)\sinh(x/\xi), \tag{8}$$

where $\xi = \frac{1}{4}\sqrt{(1+a)R_{\mathrm{cap}}^3 d_w P_b / a D_s \eta}$.

The pressure $P(x,t)$ can be found using Eq. (4) and is expressed as

$$P(x,t) = \frac{1}{a} P_b[-1 + (1+a)(\tau/\xi)A(t)\cosh(x/\xi)], \tag{9}$$

where $\tau = R_{\mathrm{cap}} d_w / 2D_s$.

Using the first boundary conditions (6), we find that

$$A(t) = \frac{\xi}{\tau \cosh[L_{\mathrm{cap}}(t)/\xi]}. \tag{10}$$

Thus, we find that the velocity distribution of liquid flux along a capillary is

$$V(x,t) = -\frac{\xi \sinh(x/\xi)}{\tau \cosh[L_{\mathrm{cap}}(t)/\xi]}, \tag{11}$$

and the pressure drop along a capillary is

$$\Delta P(x,t) = P_{\mathrm{at}} - P(x,t) = \frac{1+a}{a} P_b \left[1 + \varepsilon - \frac{\cosh(x/\xi)}{\cosh[L_{\mathrm{cap}}(t)/\xi]}\right], \tag{12}$$

where $\varepsilon = \frac{a}{1+a}\frac{2\gamma}{R_{\mathrm{cap}}} P_b \leqslant 0.05$.

B. The meniscus moving

In order to determine the displacement rate of the meniscus, the second boundary condition (6) is used

$$\frac{\partial L_{\mathrm{cap}}(t)}{\partial t} = -\frac{\xi}{\tau}\frac{\sinh[L_{\mathrm{cap}}(t)/\xi]}{\cosh[L_{\mathrm{cap}}(t)/\xi]}. \tag{13}$$

The solution of Eq. (13) is

$$\sinh[L_{\mathrm{cap}}(t)/\xi] = \sinh(L_0/\xi)\exp(-t/\tau). \tag{14}$$

At the initial stage, when $L_{\mathrm{cap}}(t)/\xi \gg 1$, Eq. (14) can be transformed into

$$\exp[L_{\mathrm{cap}}(t)/\xi] = \exp(L_0/\xi)\exp(-t/\tau). \tag{15}$$

Hence, the meniscus moves at a constant rate $-\xi/\tau$

$$L_0 - L_{\mathrm{cap}}(t) \approx \xi t/\tau. \tag{16}$$

For the opposite case, when $t/\tau \gg 1$, i.e., $L_{\mathrm{cap}}(t)/\xi \ll 1$, Eq. (14) is

$$L_{\mathrm{cap}}(t) = \xi \sinh(L_0/\xi)\exp(-t/\tau). \tag{17}$$

Hence, the meniscus displacement rate decreases exponentially,

$$V_m(t) = \frac{\partial L_{\mathrm{cap}}(t)}{\partial t} \approx -\frac{\xi}{\tau}\sinh(L_0/\xi)\exp(-t/\tau). \tag{18}$$

These solutions reflect the asymptotic behavior that is presented in Fig. 2.

Fitting a two-parameter (ξ and τ) of Eq. (14) to typical experimental data results in $\xi \approx 0.15 \times 10^{-3}$ m and $\tau \approx 1.5$ s (see Fig. 2). At the same time, the values of these parameters can be determined based on their definition [see Eqs. (8) and (9)]. Assuming that $P \approx 10^5$ Pa, $D_s \propto 5 \times 10^{-13}$ m^2/s, and $\eta \propto 100$ Pa s, we noticed that for capillaries with a radius of about $R_{\mathrm{cap}} \approx 10^{-5}$ m and a wall thickness of about $d_w \approx 0.5 \times 10^{-6}$ m, the above parameters of the model are $\xi \approx 0.35 \times 10^{-3}$ m and $\tau \approx 5$ s. Thus, the two independent methods of parameter determination result in similar values, which shows a good agreement between the suggested theoretical model and the experimental data.

V. THE POSTPROCESSES IN ELECTROSPUN TUBULAR NANOFIBER

It would appear that once the elastic energy of the fiber system increases, it tends to find another state in order to lower its energy. However, kinetic barriers can substantially influence the choices available to the system. Therefore, it is essential to explore the various possibilities that would allow the system energy to decrease.

The pressure drop across the capillary shell gives rise to a tangential stress which varies along the capillary and depends on the menisci displacement (see Fig. 5)

$$\sigma_\theta = (R_{\mathrm{cap}}/d_w)\Delta P. \tag{19}$$

This stress produces an elastic strain on the capillary shell which can result in additional postprocesses minimizing the elastic energy of the fiber shell.

A. Formation of gas bubbles

One possible means of decreasing the elastic energy of a fiber is to replace a single long slug with several smaller ones separated by areas filled both by solvent vapor and by air that has penetrated through the shell and into the fiber, i.e., the formation of gas bubbles. In order to establish the conditions

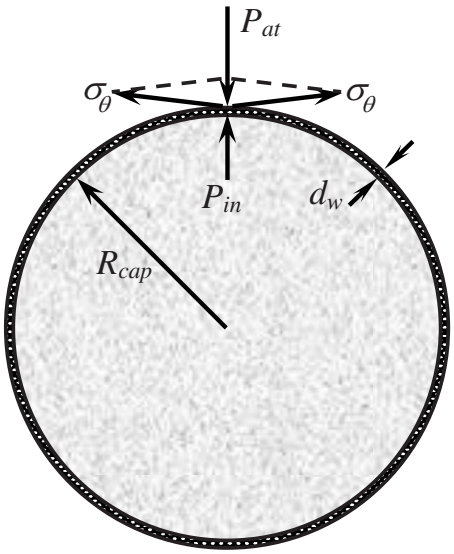

FIG. 5. The scheme of tangential stress created by the differences between the inside (P_{in}) and outside (P_{at}) pressures of a capillary, resulting in elastic compression of the capillary shell.

for bubble formation, the elastic energy of the deformed fiber shell should be determined.

The density of the elastic energy, which depends on the location along the capillary and time is $\Delta P(x,t)^2/2E$, where E is Young's modulus of the capillary shell under compression. Thus, the time-dependent elastic energy of a compressed capillary as a function of the length of the solvent slug is expressed as

$$W_{\mathrm{el}}(t) = W_{\mathrm{el}}^{(0)}\left\{\frac{L_{\mathrm{cap}}(t)}{\xi}\left[1+\frac{1}{2\cosh^2[L_{\mathrm{cap}}(t)/\xi]}\right] - \frac{3}{2}\tanh\left(\frac{L_{\mathrm{cap}}(t)}{\xi}\right)\right\}, \tag{20}$$

where $W_{\mathrm{el}}^{(0)} = (1+1/a)^2 2\pi R_{\mathrm{cap}}^3 P_b^2 \xi / E d_w$ and $L_{\mathrm{cap}}(t)$ is determined by Eq. (14).

In the case of a long slug splitting into two equal separated slugs, the elastic energy is decreasing and the energy gain can be represented as follows:

$$\Delta W_{\mathrm{el}}(L) = W_{\mathrm{el}}(L) - 2W_{\mathrm{el}}(L/2) = W_{\mathrm{el}}^{(0)} f(L/\xi), \tag{21}$$

where $f(x)$ is equal to $3[\tanh(x/2) - \tanh(x)/2] + [\cosh^{-2}(x) - \cosh^{-2}(x/2)]x/2$. If this gain of energy exceeds the energy required to create the two new menisci $2\pi R_{\mathrm{cap}}^2 \gamma$ (here $\gamma \propto 50\times 10^{-3}$ N/m is the surface tension coefficient) bubble formation takes place.

The function $\Delta W_{\mathrm{el}}(t)$ tends to a constant value 3/2 as $f(x) \approx 1.5 - 2x\exp(-x)$, if $x \gg 1$, and tends to zero as $f(x) \approx 2x^2/15$, if $x \ll 1$ (see Fig. 6). In order to find the threshold where bubble formation can occur (i.e., a slug splits into two slugs), the function $f(x)$ can be compared with the dimensionless ratio of the surface tension energy $2\pi R_{\mathrm{cap}}^2 \gamma / W_{\mathrm{el}}^{(0)} = \gamma E d_w / R_{\mathrm{cap}} P_b^2 \xi \propto 0.2$ ($E \sim 0.5$ GPa). Thus, bubble formation is possible if the length of the slug exceeds $L_{\mathrm{cap}}^{(\mathrm{cr})} \approx 1.5\xi \propto 0.3\times 10^{-3}$ m.

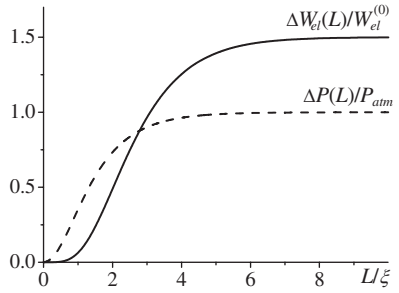

FIG. 6. The reduced gain of energy $\Delta W_{\mathrm{el}}(L)/W_{\mathrm{el}}^{(0)}$ (solid line) and the reduced pressure difference in the center of a column of liquid $\Delta P(L)/P_{\mathrm{atm}}$ (dashed line) vs reduced column length L/ξ.

This fact was confirmed by our experimental observation that within a few seconds after the fabrication of a tubular nanofiber, a large slug splits into several smaller slugs separated by gas bubbles.

B. Buckling of tubular nanofiber

However, the more interesting phenomenon is a buckling of tubular nanofiber which can occur on the final stage of solvent evaporation. Typical optical images of the buckled zones along a fiber, and the cross section of a collapsed fiber after evaporation are presented in Fig. 7. This phenomenon is related to the fact that once evaporation through the shell begins, a pressure drop across the fiber shell develops whereby the external pressure becomes higher than the internal pressure, and the tubular fiber is able to deform. It is a well known fact that for hollow cylindrical surfaces, such shape modifications are negligible if the pressure drop is relatively small; however, if this pressure drop exceeds some critical value, the cylinder becomes unstable and its shape can vary dramatically. In this case, the tubular fiber loses its structural stability and fiber buckling occurs. Taking into account the geometrical and the mechanical properties of a capillary, the critical pressure is shown to be [16]

$$\Delta P_{\mathrm{cr}} = \frac{E d_w^3}{12 R_{\mathrm{cap}}^3}\frac{n^2-1}{1-\nu^2} \propto 1.3\times 10^2 \frac{n^2-1}{1-\nu^2}\mathrm{Pa}, \tag{22}$$

where ν is the Poisson's ratio which can be taken equal to 0.5 and $n=2,3,\ldots$, is the azimuthal wave number of the buckling mode. Thus, if the pressure drop ΔP exceeds 6

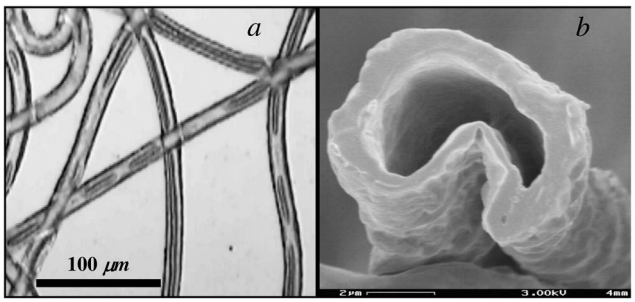

FIG. 7. Micrographs of fiber buckling: (a) the buckling zones and (b) the cross section of a collapsed fiber after evaporation.

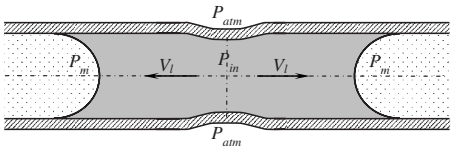

FIG. 8. A scheme of fiber buckling in the case of relatively short slugs. Due to the pressure difference $P_{\text{in}}=P_{\text{atm}}-\frac{n^2-1}{1-\nu^2}Ed_w^3/12R_{\text{cap}}^3 > P_m=P_{\text{atm}}-2\gamma/R_{\text{cap}}$, the solvent flux moves away from the buckling region.

$\times 10^2$ Pa, buckling of the capillary occurs. Therefore, based on Eq. (12), and assuming that the maximal pressure drop is at the center of the slug, we calculate that the critical length for buckling to occur when $L_{\text{cap}} > 1.1\times 10^{-2}\xi \propto 1.1 \times 10^{-6}$ m ($2L_{\text{cap}}$ is the length of the slug). Note that this length is less than the typical radius of the microtube. Consequently, the conditions that promote structural instability exist during the entire solvent evaporation process. It would seem that the conditions for fiber buckling are most favorable during the initial stage of the evaporation process when the fibers are filled with solvent and the slugs are relatively long. However, fiber buckling was observed only during the final stage of evaporation. Fortunately, there is a simple explanation for this behavior.

During the initial stage of the process, the tubular fibers are filled with solvent which prevents the fiber from buckling. Since any small deformation of a fiber would result in a decrease of the internal volume, any buckling or deformation could occur only after a portion of the solvent's volume has been removed through evaporation. This would require a flux having a direction opposite to the initial one. But this flux directional change can only occur when there is an increase in local pressure. In a region of fiber deformation the difference between the external and internal pressures sharply decreases; therefore, no further deformation or buckling of the fiber can take place.

Buckling in a filled tubular fiber is not possible when the column slug is long and the meniscus does not influence the pressure inside the fiber. However, if the slug is short enough, the surface tension forces can disturb the above stability mechanism and fiber buckling can occur. Indeed, the forces of surface tension decrease the pressure of the solvent in the meniscus region ($P_m=P_{\text{atm}}-2\gamma/R_{\text{cap}}$), so as to maintain the critical difference between external and internal pressures in a given zone of fiber deformation [$\Delta P_{\text{cr}}=P_{\text{atm}}-P_{\text{in}}$, ΔP_{cr}, is given in Eq. (22)]. At the same time, the pressure decrease provides the necessary pressure gradient along the fiber [$\Delta P_{\text{cap}}=(P_{\text{in}}-P_m)/L_{\text{cr}}$] for flux to be created by the removal of solvent with a rate exceeding that of meniscus movement (see Fig. 8). Thus, fiber buckling will take place if the following condition exists:

$$P_{\text{in}} = P_{\text{atm}} - \frac{Ed_w^3}{12R_{\text{cap}}^3}\frac{n^2-1}{1-\nu^2} > P_m = P_{\text{atm}} - \frac{2\gamma}{R_{\text{cap}}}. \quad (23)$$

The above equation demonstrates that the phenomenon of fiber buckling that can only take place during the final stage of evaporation when the slugs are sufficiently short. Assuming a Poiseuille's flow

$$V_l = \frac{R_{\text{cap}}^2}{8\eta}\frac{\Delta P_{\text{cap}}}{L_{\text{cr}}} = \frac{R_{\text{cap}}^2}{8\eta}\frac{P_{\text{in}}-P_m}{L_{\text{cr}}}$$
$$= \frac{1}{L_{\text{cr}}}\frac{R_{\text{cap}}^2}{8\eta}\left(\frac{2\gamma}{R_{\text{cap}}} - \frac{Ed_w^3}{12R_{\text{cap}}^3}\frac{n^2-1}{1-\nu^2}\right) \propto \frac{\xi}{\tau}. \quad (24)$$

The critical length of the solvent slug is calculated as

$$L_{\text{cr}} = \frac{\tau}{\xi}\frac{R_{\text{cap}}^2}{8\eta}\left(\frac{2\gamma}{R_{\text{cap}}} - \frac{Ed_w^3}{12R_{\text{cap}}^3}\frac{n^2-1}{1-\nu^2}\right) \propto 0.07\times 10^{-3}\text{m}. \quad (25)$$

This scenario was confirmed in our experimental study. During the initial stage of the evaporation process, no fiber buckling was observed. However, as the solvent evaporation progressed, regions containing no solvent began to constitute a noticeable part of the fiber. As these regions offered no resistance to fiber buckling, radial buckling was able to occur, and, indeed, was observed. The typical length of these solvent slugs was 100–200 μm or less, while the critical length as obtained in Eq. (25) was $2L_{\text{cr}} \propto 140$ μm.

VI. CONCLUSIONS

The above analysis demonstrated that despite the high evaporation rate during fabrication, coelectrospun micron-size polymer tubular structures were found to contain a significant amount of solvent. The extended period in which solvent evaporation takes place results in additional changes in the nanofiber structure. Experimental observations reveal that the solvent accumulated within the core of the fibers forms long slugs. As the remaining solvent evaporated, these slugs shortened and eventually disappeared. Direct observation showed that this process was associated with displacement of the menisci, i.e., the approximation of the ends of these slugs. The theoretical model that describes the displacement of the solvent's menisci allows one to find the correlation between the evaporation rate, the physical parameters of the nanofibers and the observed rate of meniscus displacement. The combined experimental data results in values of physical parameters of the system that are shown to be reasonable from a physical standpoint. This fact, as well as the explanation of further possible fiber evolution (bubble formation or fiber buckling), is a good verification of the proposed model and allows one to better understand the physical processes associated with solvent evaporation.

Moreover, we found that the mechanism used to explain and predict the structure evolution of the tubular nanofibers can be applied to solid-core nanofibers, as well. Indeed, the system we examined can be considered as the extreme case of the solid-core system, i.e., one with a sharp polymer density gradient (in the solid nanofiber, the polymer density near the fiber surface is high, while the polymer density in the fiber core is significantly lower [13]). Therefore, the kinetics of solvent evaporation in solid-core nanofibers is seen to be similar to that in tubular fibers. As would be expected, the rate of the process in solid-core nanofibers will be slower due to a noticeable increase in the effective viscosity of the solvent inside the fiber, which can be approximated in the initial

stage of the process by a porous medium. Nevertheless, the qualitative features of solvent evaporation in solid-core nanofibers remain inherently the same, implying that the post-processes in fabricated nanofibers, in particular, and the polymer matrix relaxation process can significantly affect the mechanical properties of polymeric nanofibers.

ACKNOWLEDGMENTS

We gratefully acknowledge the financial support by Russell Berrie Nanotechnology Institute, the Glasberg-Klein Research Fund, and the Israel Science Foundation (Grants No. 597/06 and No. 486/05).

[1] D. H. Reneker, A. L. Yarin, E. Zussman, and H. Xu, Adv. Appl. Mech. **41**, 43 (2007).
[2] D. Li and Y. N. Xia, Adv. Mater. (Weinheim, Ger.) **16**, 1151 (2004).
[3] Y. Dzenis, Science **304**, 1917 (2004).
[4] S. Ramakrishna, K. Fujihara, W.-E. Teo, T. C. Lim, and Z. Ma, *An Introduction to Electrospinning and Nanofibers*, 1st ed. (World Scientific, Singapore, 2005).
[5] A. L. Yarin, S. Koombhongse, and D. H. Reneker, J. Appl. Phys. **89**, 3018 (2001).
[6] D. H. Reneker, A. L. Yarin, H. Fong, and S. Koombhongse, J. Appl. Phys. **87**, 4531 (2000).
[7] Y. M. Shin, M. M. Hohman, M. P. Brenner, and G. C. Rutledge, Polymer **42**, 9955 (2001).
[8] M. M. Hohman, M. Shin, G. Rutledge, and M. P. Brenner, Phys. Fluids **13**, 2201 (2001).
[9] M. M. Hohman, M. Shin, G. Rutledge, and M. P. Brenner, Phys. Fluids **13**, 2221 (2001).
[10] S. A. Theron, E. Zussman, and A. L. Yarin, Polymer **45**, 2017 (2004).
[11] J. M. Deitzel, J. Kleinmeyer, D. Harris, and N. C. B. Tan, Polymer **42**, 261 (2001).
[12] S. Koombhongse, W. X. Liu, and D. H. Reneker, J. Polym. Sci., Part B: Polym. Phys. **39**, 2598 (2001).
[13] A. J. Guenthner, S. Khomobhongse, W. Liu, P. Dayal, D. H. Reneker, and T. Kyu, Macromol. Theory Simul. **15**, 87 (2006).
[14] Y. Dror, W. Salalha, R. Avrahami, E. Zussman, A. L. Yarin, A. Greiner, and J. H. Wendorff, Small **3**, 1064 (2006).
[15] Y. Peng, P. Y. Wu, and Y. L. Yang, J. Chem. Phys. **119**, 8075 (2003).
[16] S. P. Timoshenko, *Theory of Elastic Stability*, 2nd ed. (McGraw-Hill, New York, 1961).